

## Electronic Supporting Information

### **A radical photochromic metal-organic framework for boosting NIR-II photothermal conversion and therapy**

Hao Zhang,<sup>\*a</sup> Linghua Zhang,<sup>b</sup> Yue Zhong,<sup>c</sup> Jiaqi Zhou,<sup>c</sup> Yuanyuan Li,<sup>c</sup> Ping Zhang,<sup>c</sup> Junting Xi,<sup>a</sup> Wei Shi,<sup>c</sup> and Hai Qian<sup>\*a,c</sup>

*a. Department of Chemistry, School of Science, China Pharmaceutical University Nanjing, 211198, PR China.*

*b. Product Development Centre, Yichang Humanwell Pharmaceutical Co., Ltd, Yichang, 443005, PR China.*

*c. Centre of Drug Discovery, State Key Laboratory of Natural Medicines, China Pharmaceutical University, Nanjing, 210009, PR China.*

*E-mail: hzhang@cpu.edu.cn, qianhai24@163.com*

# 1. Experimental section

## 1.1 Materials and methods

All chemicals, biological reagents and solvents used for synthesis were obtained from commercial sources and were used as received, without further purification unless specified. All reactions were carried out under aerobic conditions. Water used in this work was triple distilled. CCK-8 and Calcein AM/PI Apoptosis Detection Kits were purchased from Beyotime Biotechnology. Annexin V-FITC/PI Apoptosis Detection Kit was purchased from Vazyme Biotechnology. The Mice breast cancer cells (4T1) were obtained from ATCC and cultured in an incubator with a humidified atmosphere of 5% CO<sub>2</sub> at 37 °C. The ligand PTIA was prepared according to literature procedures (Scheme S1, ESI†).<sup>1</sup>

Elemental analyses (C, H and N) were performed on a ELEMENTAR VARIO elemental analyzer. IR spectra were measured on a Nicolet 6700 spectrometer with KBr pellets in the range of 4000–400 cm<sup>-1</sup>. Thermal stability was determined by thermogravimetry (TG) and derivative with a heating rate of 10 K min<sup>-1</sup> under a nitrogen atmosphere. Powder X-ray diffraction (PXRD) was recorded on a Rigaku SmartLab (3 kW) X-ray diffractometer with a Cu sealed tube. Transmission electron microscopy (TEM) images were observed using a FEI/Philips Tecnai 12 BioTWIN. Size of nanoparticles analysis measurements were recorded using a Dynamic Light Scattering Particle Size Analyzer (Malvern Zetasizer Nano ZS). Solid-state UV-Vis-NIR spectroscopy were determined on a SHIMADZU UV-3600 spectrometer. BaSO<sub>4</sub> plates were used as references (100% reflection), on which the finely ground power of a sample was coated. Electron spin resonance (ESR) spectra were recorded on a Bruker Elexsys II E500 spectrometer using powder samples in a 100 G/s sweep speed at a frequency of 9.84 GHz and at room temperature. X-ray photoelectron spectroscopy (XPS) studies were performed with a ThermoFisher Scientific ESCALAB 250 Xi spectrometer using Al K $\alpha$  radiation ( $\lambda = 8.357 \text{ \AA}$ ), and the C1s line at 284.8 eV was used as the binding energy reference. The ultrasonic dispersion treatment was performed on a YUNYI YA008C ultrasonic cleaner (40 KHz, 360 W). A MingRen ZF-5 ultraviolet analyzer (365 nm, 12 W) was used for UV irradiation experiments, and the distance between the sample and the lamp was around 10 cm. The UV-irradiated time to prepare pMOF-a is 30 mins. For the photothermal experiments, the diode pumped solid-state laser (1064 nm, continuous wave, VLC-1064nmM0-2W, BLUEPRINT, China) was used as the excitation light source and the thermal images were recorded by a FLIR Infrared Camera (model: FLIR One Pro). Confocal laser scanning microscope (CLSM) images were performed on Olympus FV3000 confocal laser scanning microscope. Flow cytometry assays was performed by BD Accuri C6 Plus flow cytometer, and analyzed by Flowjo Software.

## 1.2 Synthesis of pMOF

Zn(NO<sub>3</sub>)<sub>2</sub>·6H<sub>2</sub>O (29.8 mg, 0.1 mmol) and 2,4,6-tri(4-pyridyl)-1,3,5-triazine (15.5 mg, 0.05 mmol) were dissolved into water (5 mL) and stirred for 0.5 h. The transparent solution was then added into the H<sub>3</sub>PTIA aqueous solution (38.4 mg, 0.05 mmol in 5 mL of water), which was firstly adjusted to an acidity of pH 5.5 with 1 M NaOH aqueous solution. After stirred for 10 min, the mixture was then transferred to and sealed in a Teflon reactor (20 mL) and heated at 140 °C for 72 h. After that the mixture was cooled to 30 °C. at about 5 °C h<sup>-1</sup>. Pale yellow prismatic crystals used for the X-ray diffraction determination were obtained by filtration and washed with DMF. Yield: 68.1% based on H<sub>3</sub>PTIA. Elemental analysis calcd (%) for C<sub>62</sub>H<sub>66</sub>N<sub>24</sub>O<sub>25</sub>Zn<sub>4</sub>: C, 41.16; H, 3.68; N, 18.53; found: C, 41.55; H, 3.67; N, 18.25.

## 1.3 Preparation of pMOF and pMOF-a NPs

The nanoparticles of pMOF and pMOF-a were prepared via matrix-encapsulation method.<sup>2,3</sup> In brief, the as-

prepared crystals were grounded into the powder with a quartz mortar and pestle. The powder pMOFs (10.3 mg) and Pluronic F127 (40 ~ 50 mg) were dissolved in CH<sub>3</sub>OH (50 ml). the mixture was evenly disposed by ultrasonic dispersion at room temperature for 2 h and dried over under vacuum to remove CH<sub>3</sub>OH. After that, the colourless lipidic film containing pMOF NPs can be obtained.

#### **Preparation of pMOF NPs**

10 mL of water or PBS solution was added in to the obtained lipidic film, and the solution was kept by sonication for 20 min and further stirred in the dark for 2 h. The nanoparticles suspension was obtained and stored at 4 °C for further use.

#### **Preparation of pMOF-a NPs**

After irradiated for 30 mins under an ultraviolet analyzer (365 nm, 12 W), the black lipidic film was prepared where pMOF NPs were transformed into pMOF-a NPs. 10 mL of water or PBS solution was added in to this lipidic film containing pMOF-a NPs, and the solution was kept by sonication for 20 min and further stirred in the dark for 2 h. The nanoparticles suspension was obtained and stored at 4 °C for further use.

### **1.4 X-ray Crystallographic Study**

The suitable single crystal of pMOF was mounted on a glass rod for the determination of crystal structure. X-ray diffraction data collection was performed on a Bruker SMART APEX II diffractometer with a CCD area detector and graphite-monochromated Cu *K* $\alpha$  ( $\lambda = 1.54184 \text{ \AA}$ ) radiation sources at 293 K. Multi-scan absorption corrections were applied using the *SADDABS* program (Bruker, 2016/2). Using *OLEX2* (Dolomanov *et al.*, 2009)<sup>4</sup>, the structure was solved by intrinsic phasing employing *ShelXT* (Sheldrick, 2015)<sup>5</sup> and refined with the *shelXL* (Sheldrick, 2015)<sup>6</sup> package, using the full-matrix least-squares method on  $F^2$ . Non-H atoms were refined anisotropically. H atoms were mostly included at geometrically calculated positions with displacement parameters derived from the parent atoms. H atoms attached to the coordinated water molecules or to groups suitable for forming hydrogen bonds were located on Fourier maps, and refined using isotropic displacement parameters depending on the parent atoms. Crystal data collection and structure refinement details are summarized in Table S1. More details on the crystallographic studies as well as atomic displacement parameters are given in Supporting Crystallographic Data as CIF files.

### **1.5 Photothermal effect and PCE calculation**

#### **Photothermal conversion measurement**

For the purpose of evaluating the photothermal ability of pMOF-a NPs, first, we discussed the effect of power density on conversion efficiency. pMOF-a NPs aqueous solution (1 mg mL<sup>-1</sup>) were irradiated by 1064 nm laser at different power densities (0.5 W cm<sup>-2</sup>, 0.75 W cm<sup>-2</sup>, 1 W cm<sup>-2</sup>, 1.25 W cm<sup>-2</sup> and 1.5 W cm<sup>-2</sup>). The temperature changes were monitored by FLIR One Pro thermal camera. Next, we considered the effect of concentration on temperature. Different concentrations of pMOF-a NPs aqueous solution were prepared (0.25 mg mL<sup>-1</sup>, 0.5 mg mL<sup>-1</sup>, 1 mg mL<sup>-1</sup> and 2 mg mL<sup>-1</sup>), and irradiated by 1 W cm<sup>-2</sup> with 1064 nm laser for 12 min. The temperature changes were monitored during irradiation. Finally, the sample solution (1 mg mL<sup>-1</sup>) was irradiated by 1 W cm<sup>-2</sup> with 1064 nm laser for six cycles of on-off processes, each composed of a heating period of 12 min and a natural cooling period, to further test the photothermal stability.

#### **Calculation of photothermal conversion efficiency**

The photothermal conversion efficiency ( $\eta$ ) of pMOF NPs and pMOF-a NPs was calculated according to the previously reported methods,<sup>7</sup> detailed calculation of pMOF-a NPs as an example was listed:

During the photothermal heating process, the total energy balance for the system can be expressed as:

$$\sum_i m_i C_{p,i} \frac{d\Delta T}{dt} = Q_{NP} + Q_S - Q_{Loss} \quad (1)$$

Where  $m$  (g) represents the mass of the solution ( $m_s$ ) and sample cuvette ( $m_q$ ),  $C$  (J/g °C) includes the constant-pressure heat capacity of solution ( $c_s$ ) and sample cuvette ( $c_q$ ),  $\Delta T$  (°C) is the difference between the solution temperature  $T$  at time  $t$  and the starting solution temperature  $T_0$ ,  $Q_{NP}$  (mW) is determined as the energy arising from the nanoparticles, and  $Q_{Loss}$  (mW) is the thermal energy lost to the surrounding environment. In addition,  $Q_S$  (mW) is the energy input by the sample cuvette and the solvent (pure DI water).

For  $Q_{NP}$ , the following equation can be given as:

$$Q_{NP} = I(1 - 10^{-A_{1064}})\eta \quad (2)$$

Where  $I$  is the laser power which is incident on the system,  $A_{1064}$  is defined as the absorbance of pMOF-a NPs at the wavelength of 1064 nm, and  $\eta$  is known as the photothermal conversion efficiency from the absorbed laser energy to thermal energy. Furthermore, the energy dissipation mainly occurs through the heat conduction and thermal radiation.  $Q_{Loss}$  is linear with temperature for the outgoing thermal energy, then take the form as:

$$Q_{Loss} = hS\Delta T = hS(T - T_{Sur}) \quad (3)$$

Where  $h$  (mW/(m<sup>2</sup>·°C)) is heat transfer coefficient,  $S$  (m<sup>2</sup>) is the surface area of the container,  $\Delta T$  is the temperature change which is defined as  $T - T_{Sur}$ ,  $T$  (°C) is the water temperature and  $T_{Sur}$  (°C) is the solution temperature ambient temperature of surrounding environment.

When the temperature rises at a maximum steady-state temperature  $T_{Max}$  (°C), the system reaches the steady state. In this case, the heat input is equal to heat output, and the left side of (1) become zero. We then obtain

$$Q_{NP} + Q_S = Q_{Loss} = hS(T_{Max} - T_{Sur}) \quad (4)$$

Then  $\eta$  can be determined by combining the previous equations and rearranging:

$$\eta = [hS(T_{Max} - T_{Sur}) - Q_S] / I(1 - 10^{-A_{1064}}) \quad (5)$$

Where  $Q_S$  is measured independently according to (11), the  $(T_{Max} - T_{Sur})$  is 25.70 °C,  $I$  is 1000 mW,  $A_{1064}$  is 0.560 (Figure S17). Thus, in the above equation, only the  $hS$  remains unknown parameter for calculating  $\eta$ .

In order to solve  $hS$ , the following notation  $\theta$  is used herein, which is defined as the ratio of  $(T - T_{Sur})$  to  $(T_{Max} - T_{Sur})$ :

$$\theta = (T - T_{Sur}) / (T_{Max} - T_{Sur}) \quad (6)$$

And a sample system time constant  $\tau_s$  (s) is introduced:

$$\tau_s = \frac{\sum_i m_i C_{p,i}}{hS} \quad (7)$$

Substituting (2), (3), (6) and (7) into (1) and rearranging to obtain:

$$\frac{d\theta}{d\tau} = \frac{1}{\tau_s} \left[ \frac{Q_{NP} + Q_S}{hS(T_{max} - T_{Sur})} - \theta \right] \quad (8)$$

When at the cooling stage, the laser source has been shut off, so the  $Q_{NP} + Q_S = 0$ . Under this condition, we can obtain:

$$dt = -\tau_s (d\theta / \theta) \quad (9)$$

After integrating the equation (10), we can obtain:

$$t = -\tau_s \ln \theta \quad (10)$$

Therefore, time constant for heat transfer from the system of pMOF-a NPs is determined to be  $\tau_s = 193.72$  s by applying the linear time data from the cooling period vs  $-\ln\theta$  (Figure S20). In addition, the  $m$  is 0.5 g and the  $c$  is 4.2 J/g °C. Thus, according to (7), the  $hS$  is calculated to be 10.84 mW/°C.

$$Q_S = \frac{c m (T_{Max(water)} - T_{Surr})}{\tau_{s(water)}} \quad (11)$$

Where  $T_{max(water)} - T_{Surr}$  is 5.1 °C and  $\tau_{s(water)}$  is 236.2 s; thus,  $Q_S$  was calculated to be 45.3 mW. Substituting all the obtained data into (4), the result photothermal conversion efficiency ( $\eta$ ) of pMOF-a NPs can be calculated to be 32.2%.

Taking a similar approach, we can obtain time constant for heat transfer from pMOF NPs:  $\tau_s = 204.04$  s (Figure S21). according to (7), the  $hS$  of pMOF NPs is calculated to be  $10.29$  mW/°C. Besides, the  $(T_{Max}-T_{Sur})$  of pMOF NPs is  $8.4$  °C,  $I$  is  $1000$  mW,  $A_{1064}$  is  $0.038$  (Figure S17). Substituting all the obtained data into (4), the result photothermal conversion efficiency ( $\eta$ ) of pMOF-a NPs can be calculated to be  $49.1\%$ .

## 1.6 Cell experiment

### Cell culture

Mice breast cancer cells (4T1 cell lines) were cultured in Dulbecco's modified Eagle's medium (DMEM) containing 10% fetal bovine serum (FBS),  $100 \mu\text{g mL}^{-1}$  streptomycin and  $100 \text{ U mL}^{-1}$  penicillin at  $37$  °C in a humidified incubator containing 5%  $\text{CO}_2$  and 95% air. The medium was replenished every other day and the cells were sub-cultured after reaching confluence.

### Cell Viability Assay

We evaluated the inhibition rates of pMOF NPs and pMOF-a NPs with/without irradiation by a Cell Counting Kit-8 (CCK-8) assay in vitro. The cells were planted in 96-well plates at a density of 6000 cells per well in  $100 \mu\text{L}$  of complete medium. After incubation for 24 h, they were subjected to six different treatments: PBS control group (group 1), treatment with 1064 nm laser irradiation only (group 2), incubated with pMOF NPs PBS solution at certain concentrations (group 3), incubated with pMOF NPs PBS solution and then irradiation (group 4), incubated with pMOF-a NPs PBS solution at certain concentrations (group 5), incubated with pMOF-a NPs PBS solution at certain concentrations and then irradiation (group 6). After 4 hours of adding respective solution, NIR-II laser (1064 nm) irradiation was performed on group 2, 4 and 6 at  $1 \text{ W cm}^{-2}$  for 5 min. After the laser irradiation, the medium was replaced with DMEM and then incubated for another 4 hours under 5%  $\text{CO}_2$  atmosphere at  $37$  °C. CCK-8 solution was added to every well and left for 2 h. A microplate reader (Bio-Rad) was used to record the absorption at 450 nm. Six independent experiments were performed.

### Confocal Laser Scanning Microscopy

4T1 cells were seeded onto 35 mm confocal dishes for 24 h, then cells were treated with following treatments: PBS, cells were incubated without any treatments; PBS+1064 nm, cells were irradiated with 1064 nm laser irradiation ( $1 \text{ W cm}^{-2}$ ) for 5 min; pMOF NPs, cells were incubated with  $1.0 \text{ mg mL}^{-1}$  pMOF NPs PBS solution at  $37$  °C for 4 h; pMOF NPs+1064 nm, cells were incubated with  $1.0 \text{ mg mL}^{-1}$  pMOF NPs PBS solution at  $37$  °C for 4 h, and followed by 1064 nm laser irradiation ( $1 \text{ W cm}^{-2}$ ) for 5 min; pMOF-a NPs, cells were incubated with  $1.0 \text{ mg mL}^{-1}$  pMOF NPs PBS solution at  $37$  °C for 4 h; pMOF-a NPs+1064 nm, cells were incubated with  $1.0 \text{ mg mL}^{-1}$  pMOF NPs PBS solution at  $37$  °C for 4 h, and followed by 1064 nm laser irradiation ( $1 \text{ W cm}^{-2}$ ) for 5 min. After incubation for 4 h, cells were stained with Calcein AM/PI Apoptosis Detection Kit according to the manufacture instruction, and imaged by a confocal laser scanning microscopy (Olympus FV-3000). Calcein AM was excited with a 488 nm laser, detected in the range from 500 to 540 nm; PI was excited with a 488 nm laser, detected in the range from 653 to 690 nm.

### Apoptosis/Necrosis Assay

4T1 cells were seeded onto 35 mm confocal dishes for 24 h, then cells were treated with following treatments: PBS, cells were incubated without any treatments; PBS+1064 nm, cells were irradiated with 1064 nm laser irradiation ( $1 \text{ W cm}^{-2}$ ) for 5 min; pMOF NPs, cells were incubated with  $1.0 \text{ mg mL}^{-1}$  pMOF NPs PBS solution at  $37$  °C for 4 h; pMOF NPs+1064 nm, cells were incubated with  $1.0 \text{ mg mL}^{-1}$  pMOF NPs PBS solution at  $37$  °C for 4 h, and followed by 1064 nm laser irradiation ( $1 \text{ W cm}^{-2}$ ) for 5 min; pMOF-a NPs, cells were incubated

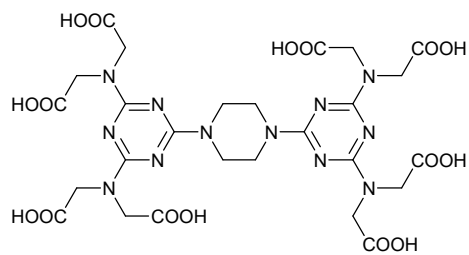
with 1.0 mg mL<sup>-1</sup> pMOF NPs PBS solution at 37 °C for 4 h; pMOF-a NPs+1064 nm, cells were incubated with 1.0 mg mL<sup>-1</sup> pMOF NPs PBS solution at 37 °C for 4 h, and followed by 1064 nm laser irradiation (1 W cm<sup>-2</sup>) for 5 min. After incubation for 4 h, cells were stained with Annexin V/PI Apoptosis Detection Kit for 15 min. Finally, the cells of different experimental groups were collected and quantified with a flow cytometer.

## 2. Characterization Results

Table S1. Crystallographic data collection and refinement result for pMOF.

Temperature	293 K
Empirical formula	C <sub>62</sub> H <sub>66</sub> N <sub>24</sub> O <sub>25</sub> Zn <sub>4</sub>
Formula weight	1808.86
Crystal system	monoclinic
Space group	<i>P2<sub>1</sub></i>
<i>a</i> (Å)	9.8273(4)
<i>b</i> (Å)	32.5702(10)
<i>c</i> (Å)	11.6532(4)
$\alpha$ (°)	90
$\beta$ (°)	101.048(4)
$\gamma$ (°)	90
<i>V</i> (Å <sup>3</sup> )	3660.8(2)
<i>Z</i>	2
<i>D<sub>c</sub></i> (g/cm <sup>3</sup> )	1.641
$\mu$ (mm <sup>-1</sup> )	2.323
<i>F</i> (000)	1852.0
$\theta$ range (°)	5.426 - 133.162
<i>R</i> (int)	0.0336
<i>R<sub>1</sub></i> , <sup>a</sup> <i>wR<sub>2</sub></i> <sup>b</sup> ( <i>I</i> > 2σ( <i>I</i> ))	0.0518, 0.1359
GOF on <i>F</i> <sup>2</sup>	1.051
Flack parameter	0.44(4)

<sup>a</sup>  $R_1 = \Sigma(|F_o| - |F_c|) / \Sigma|F_o|$ , <sup>b</sup>  $wR_2 = \{[\Sigma w[(F_o^2 - F_c^2)^2] / \Sigma w(F_o^2)^2]\}^{1/2}$ .



**Scheme S1.** Structure of ligand H<sub>8</sub>PTIA.

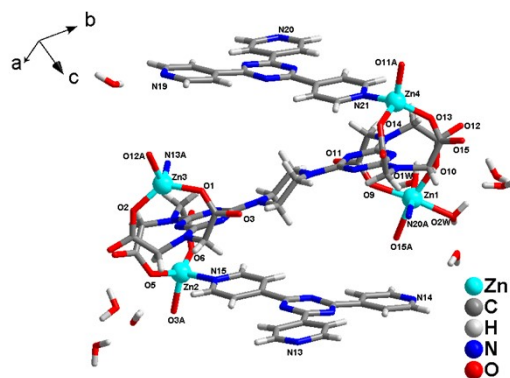


**Figure S1.** The asymmetric unit of pMOF.

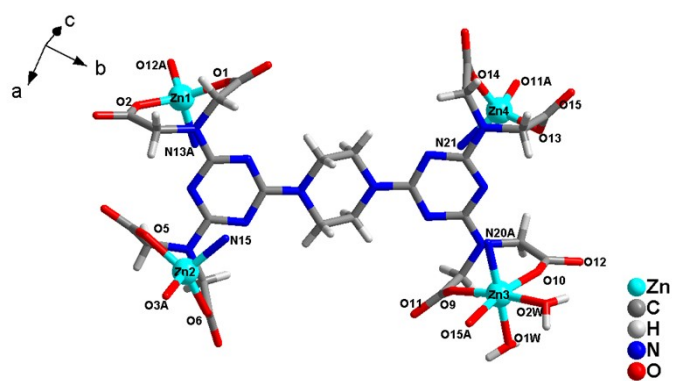


**Figure S2.** The coordination environment of PTIA<sup>8-</sup>.

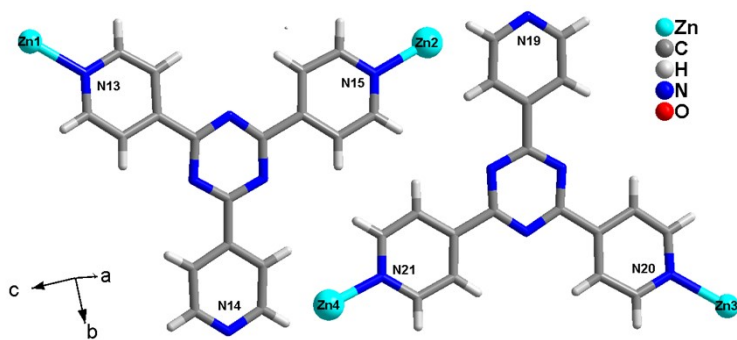


**Figure S3.** The coordination environment of the TPT ligands.

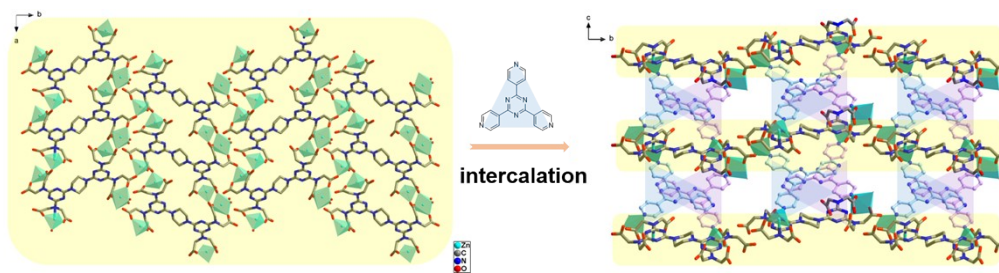


**Figure S4.** The 2D layer structure of pMOF viewed along the c-axis (left) and the 3D framework along a axis (right).

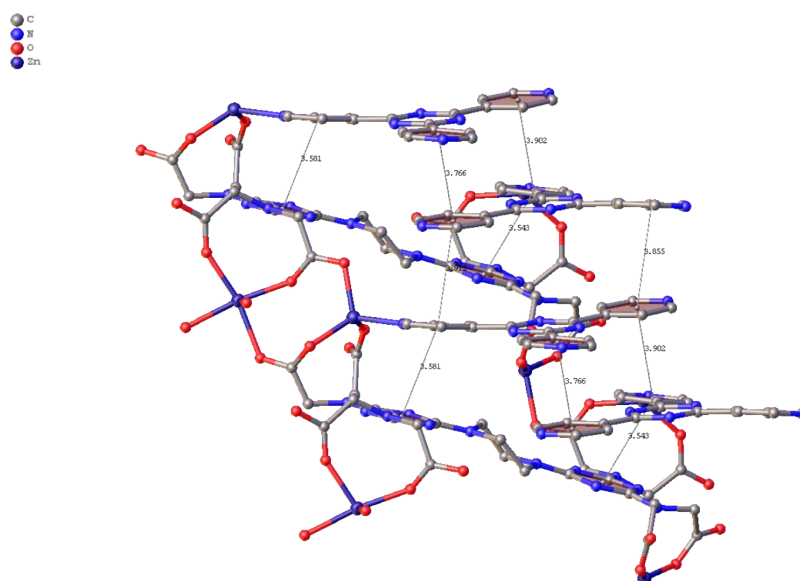


**Figure S5.**  $\pi$ - $\pi$  and D-A interactions between PTIA and TPT ligands.

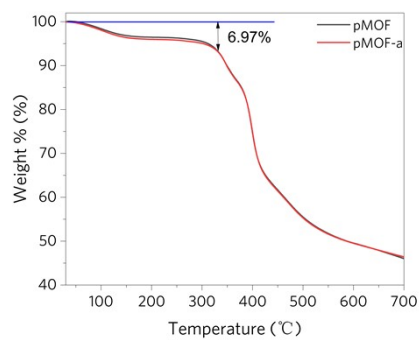


**Figure S6.** Thermogravimetric curve of pMOF and pMOF-a.

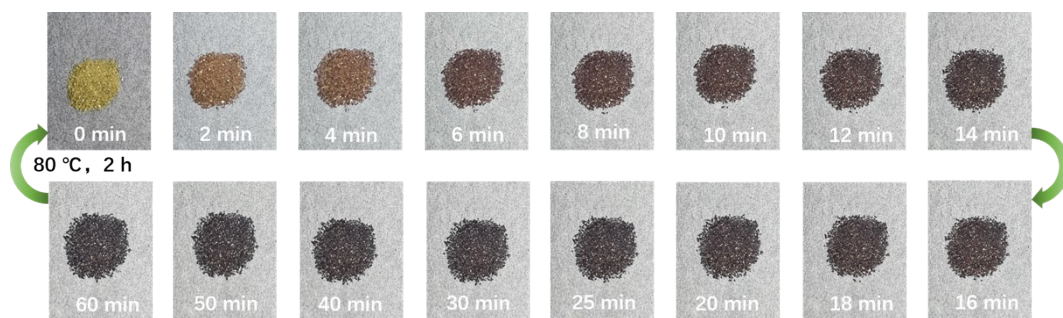


**Figure S7.** Reversible photochromic phenomenon of pMOF upon irradiated by an extra UV lamp (365 nm, lamp power: 12 W).

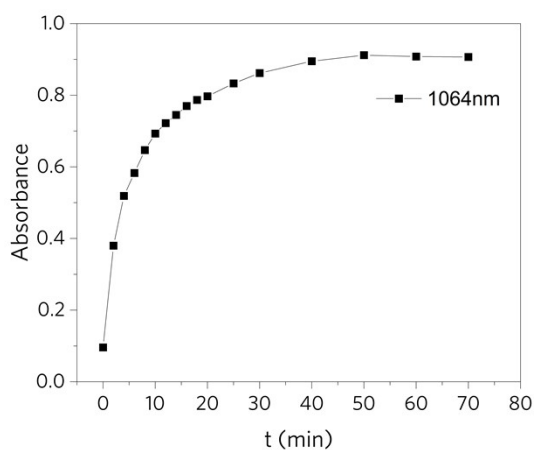


**Figure S8.** Time-dependent absorption peak at 1064 nm of pMOF upon UV irradiation via the solid-state UV-Vis-NIR absorption spectra.

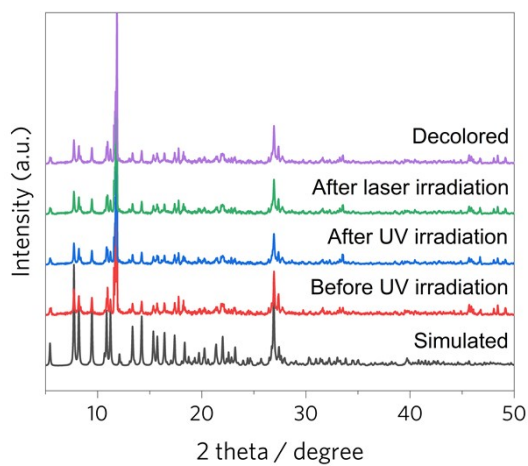


**Figure S9.** Simulated and experimental PXRD patterns for pMOF before UV irradiation, after UV irradiation, after 1064 nm laser irradiation and decoloured.

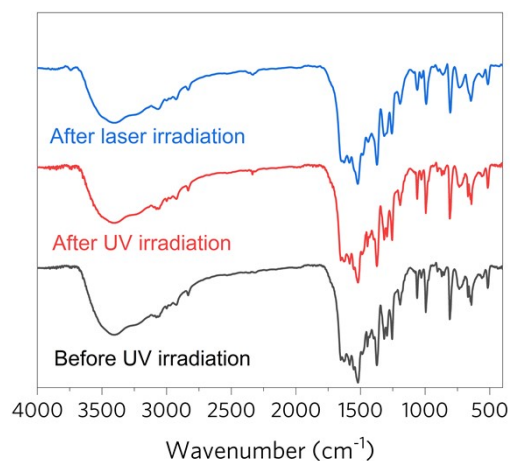


**Figure S10.** The FT-IR spectra for pMOF before UV irradiation, after UV irradiation and after 1064 nm laser irradiation.

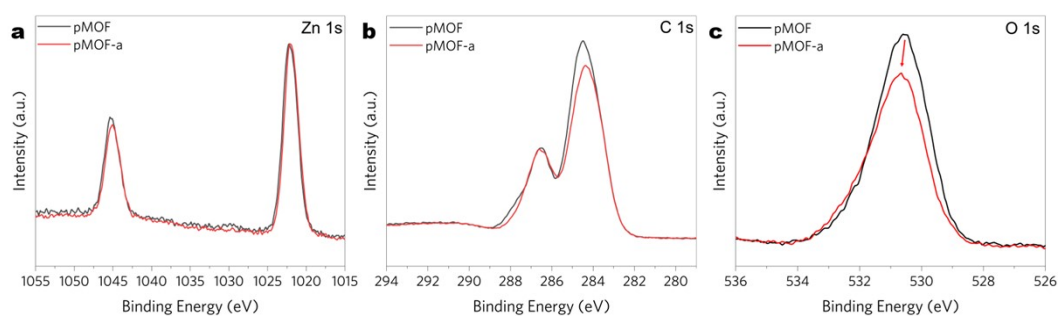


**Figure S11.** XPS core-level spectra of pMOF before and after UV irradiation

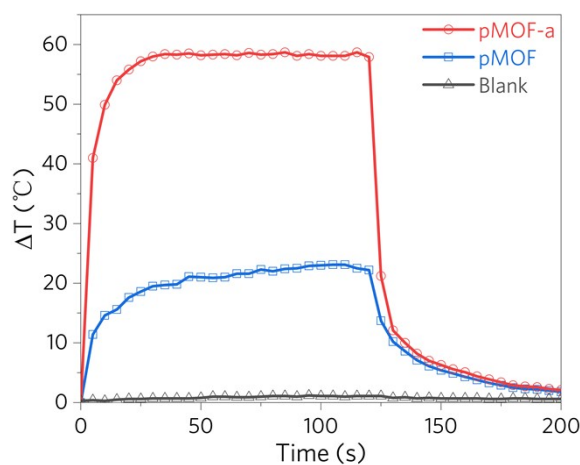


**Figure S12.** Photothermal conversion of pMOF film on quartz glass under NIR-II laser irradiation (1064 nm, 1  $\text{W cm}^{-2}$ ).

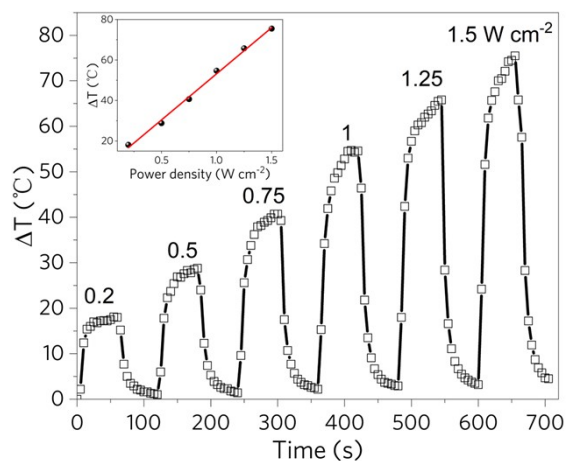


**Figure S13.** Temperature changes of pMOF-a film at different NIR-II laser intensities. Inset shows temperature changes as a function of NIR-II laser intensities.

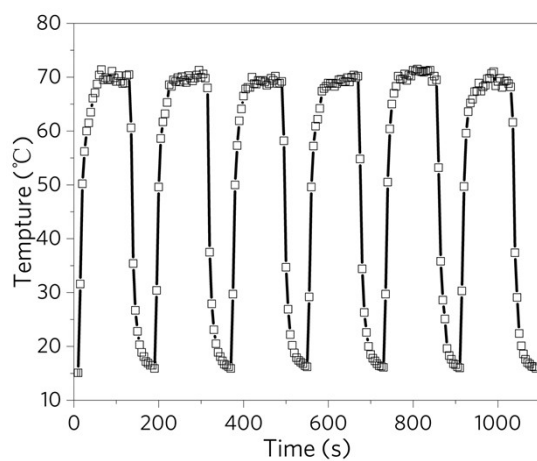


**Figure S14.** Temperature evolutions of pMOF-a before and after 5 heating/cooling cycles under 1064 nm laser irradiation ( $1.5 \text{ W cm}^{-2}$ )

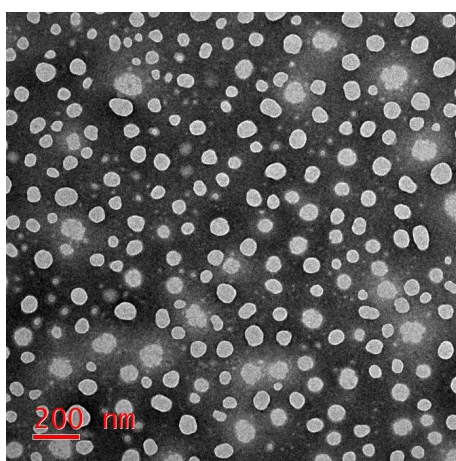


**Figure S15.** TEM image of pMOF-a NPs in water.

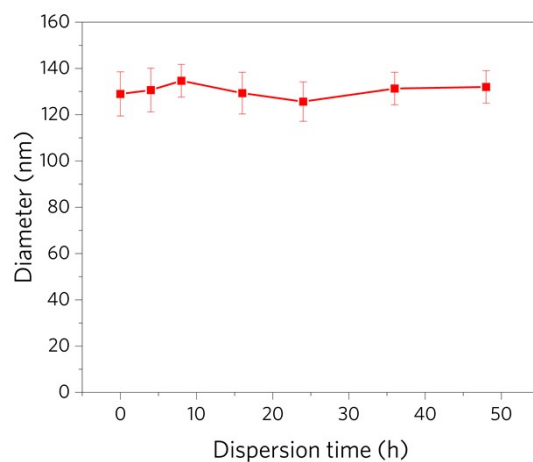


**Figure S16.** The dispersion stability of pMOF-a NPs aqueous solution measured over 48 hours via dynamic light scattering (DLS) analysis.

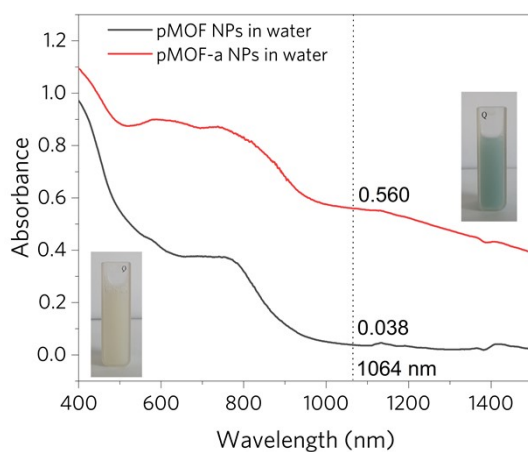


**Figure S17.** The NIR absorption spectra of pMOF NPs and pMOF-a NPs in water (1 mg/mL).

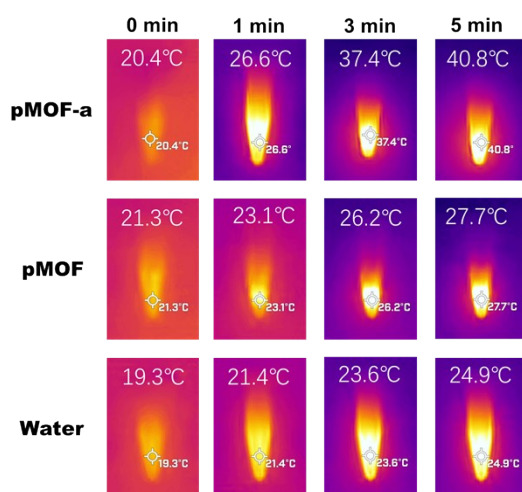


**Figure S18.** Photothermal image of water and the aqueous solutions of pMOF and pMOF-a NPs at the concentration of 1 mg mL<sup>-1</sup> under NIR-II laser irradiation (1064 nm, 1 W cm<sup>-2</sup>).

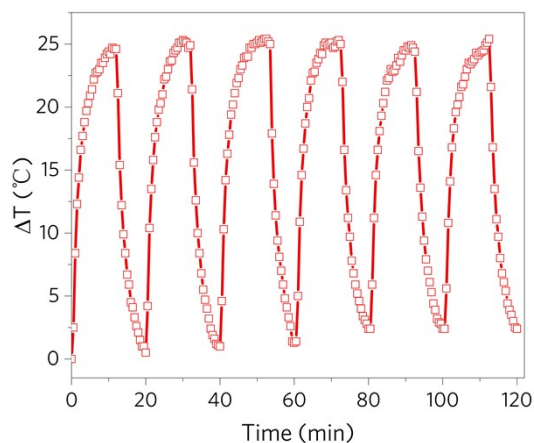


**Figure S19.** Photothermal stability study of pMOF-a NPs aqueous solution ( $1 \text{ mg mL}^{-1}$ ,  $1064 \text{ nm}$ ,  $1 \text{ W cm}^{-2}$ ) during six cycles of heating cooling processes.

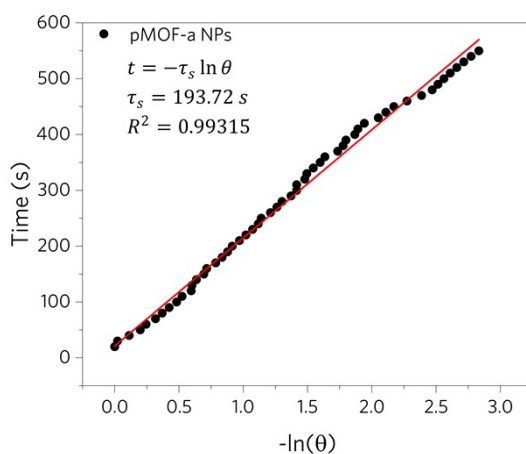


**Figure S20.** The plots of time versus  $-\ln(\theta)$  from the data recorded during the cooling period (Fig. 3b) of the experiments for pMOF-a NPs. The slopes can be used to calculate  $\tau_s$  and PCE ( $\eta$ ).

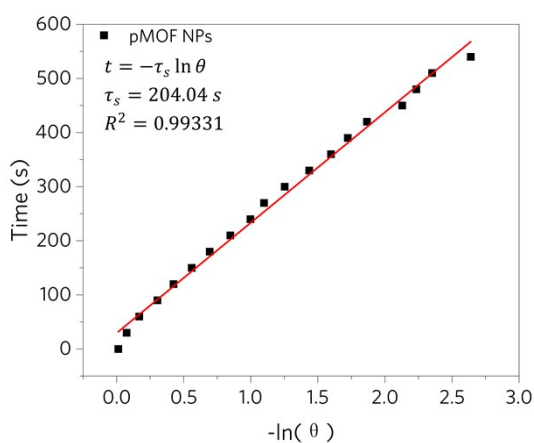


**Figure S21.** The plots of time versus  $-\ln(\theta)$  from the data recorded during the cooling period of the experiments for pMOF NPs. The slopes can be used to calculate  $\tau_s$  and PCE ( $\eta$ ).

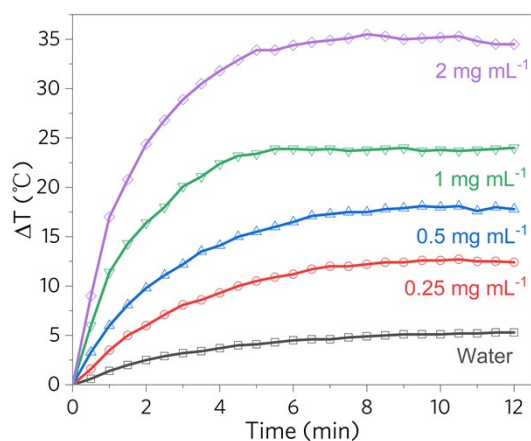


**Figure S22.** Photothermal conversion of pMOF-a NPs aqueous solution at different concentrations.

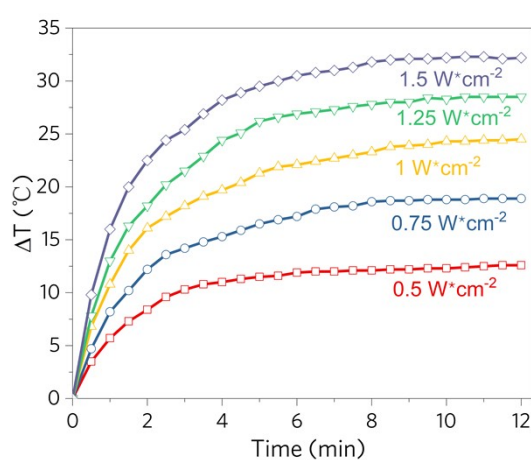


**Figure S23.** Photothermal conversion of pMOF-a NPs aqueous solution (1 mg mL<sup>-1</sup>) under 1064 nm laser irradiation with different exposure intensity (0.5 – 1.5 W cm<sup>-2</sup>).

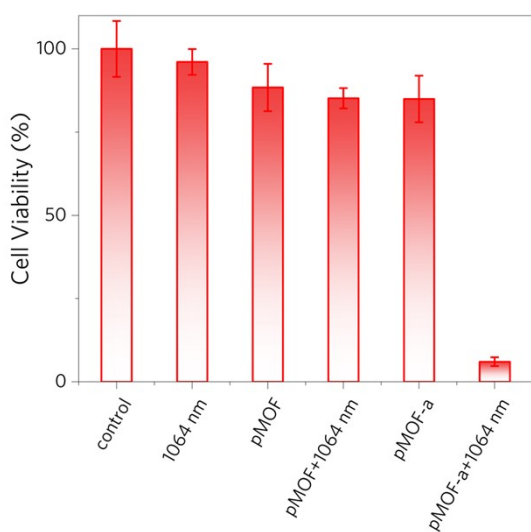


**Figure S24.** The cell viability of Cell viability of 4T1 cells after different treatment. The 1064 nm irradiation was fixed at 1 W cm<sup>-2</sup> and the irradiation times were 5 min. The loading of pMOF NPs and pMOF-a NPs was 1 mg mL<sup>-1</sup> in PBS solution.

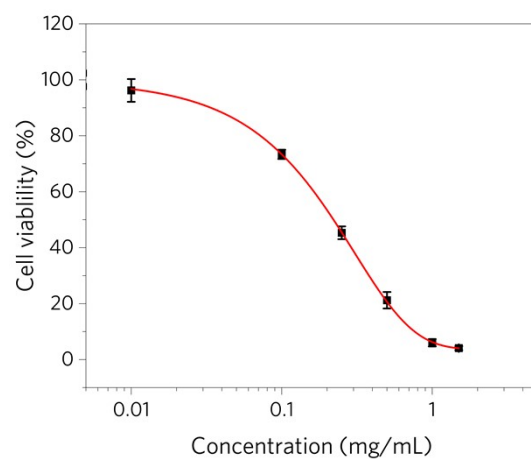


**Figure S25.** The cell viability of 4T1 cells at the concentration range of 0 ~ 1.5 mg/mL for pMOF-a NPs aqueous solution under 1064 nm laser illumination (1 W/cm<sup>2</sup>).

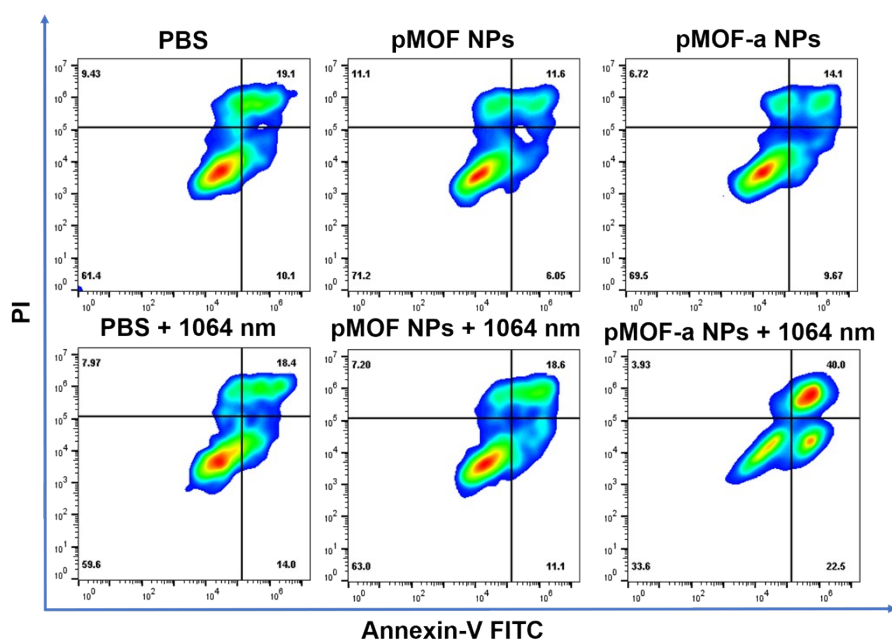


**Figure S26.** annexin V-FITC/PI analyses of 4T1 cells after different treatments. The 1064 nm irradiation was fixed at 1 W cm<sup>-2</sup> and the irradiation times were 5 min. The loading of pMOF NPs and pMOF-a NPs was 1 mg mL<sup>-1</sup> in PBS solution.

## references

- 1 H. Zhang and X. Wu, *Adv. Sci.*, 2016, **3**, 1500224.
- 2 J. S. Suk, Q. Xu, N. Kim, J. Hanes and L. M. Ensign, *Adv. Drug Deliv. Rev.*, 2016, **99**, 28–51.
- 3 J. Li and K. Pu, *Chem. Soc. Rev.*, 2019, **48**, 38–71.
- 4 O. V. Dolomanov, L. J. Bourhis, R. J. Gildea, J. A. K. Howard and H. Puschmann, *J. Appl. Crystallogr.*, 2009, **42**, 339–341.
- 5 G. M. Sheldrick, *Acta Crystallogr. Sect. Found. Adv.*, 2015, **71**, 3–8.
- 6 G. M. Sheldrick, *Acta Crystallogr. Sect. C Struct. Chem.*, 2015, **71**, 3–8.
- 7 S. Lei, F. Zhao, J. Zhang, N. T. Blum, T. He, J. Qu, P. Huang and J. Lin, *Anal. Chem.*, 2022, **94**, 8399–8408.